

# TwoSpect: tuning up to search for gravitational waves from Scorpius X-1

Grant David Meadors<sup>1</sup>, Evan Goetz<sup>2</sup>, Keith Riles<sup>2</sup>

<sup>1</sup>Max-Planck-Institut für Gravitationsphysik, Am Mühlenberg 1, 14476 Potsdam and Callinstraße 38, 30167 Hannover, Germany

<sup>2</sup>University of Michigan, 450 Church Street, Ann Arbor, Michigan 48109, USA

E-mail: `grant.meadors@aei.mpg.de`

**Abstract.** We describe the tuning of the TwoSpect data analysis method to search for continuous gravitational waves from sources such as the Low Mass X-ray Binary, Scorpius X-1. TwoSpect sensitivity is enhanced when the source sky location and period are known. Simulations of the orbital and gravitational-wave parameters of Scorpius X-1 have already been made in the context of a comparison of search algorithms. These simulations are here used to quantify the sensitivity enhancement and parameter estimation abilities of this tuned, directed TwoSpect method. The gravitational wave strain, gravitational wave frequency, and projected semi-major axis of the binary system are recovered and uncertainty estimated, for simulated signals that are detected. Upper limits on gravitational wave strain are set for undetected signals. Applications to future searches in gravitational-wave interferometer data are discussed. Directed TwoSpect searches analyze gravitational-wave data for signals from LMXBs; robust against spin-wandering and computationally tractable for unknown signal frequency, this directed search method is an important tool to analyze interferometer detector data.

PACS numbers: 04.30.-w, 04.30.Tv, 04.40.Dg, 95.30.Sf., 95.75.Pq, 95.85.Sz, 97.60.Jd

## 1. Introduction

Continuous gravitational waves from neutron stars in binary systems seem likely to be one of the most interesting types detectable by ground-based interferometric observatories. Binary systems constitute 237 of 578 (44%) of known pulsars in the ATNF catalog (v1.53, 2015) [1] with rotational frequency faster than 5 Hz, which is approximately the lower bound of the frequency range of Advanced LIGO and Advanced Virgo [2, 3]. TwoSpect [4, 5] is one data analysis method for targeting these systems. This method can apply to continuous gravitational waves of unknown frequencies from neutron stars in binary systems, with unknown sky locations, orbital periods, or projected semi-major axes. TwoSpect was used in a prior all-sky search for continuous gravitational waves from unknown neutron stars in binary systems with data from LIGO Science Run 6 and Virgo Science Runs 2 and 3 [6]. This paper

describes analysis modifications, when sky location and orbital period are known, to run a *directed* search that is more sensitive than the all-sky method. Scorpius X-1 (Sco X-1) is a prototypical source, for which these changes are demonstrated in an algorithm comparison [7].

Gravitational-wave (GW) analyses for continuous-wave (CW) signals from isolated neutron stars are computationally-demanding [8] but conceptually simple. Time-varying mass quadrupole moments, such as ellipticity in a star, could induce CW emission, as could stellar *r*-modes [9, 10]. When these emissions, with a strain amplitude  $h_0$  and a phase evolution described in Section 2, arrive at a GW observatory, they may be very faint. CW analysis methods include the  $\mathcal{F}$ -statistic, Hough, StackSlide and PowerFlux methods [11–16]. Many stars, possibly the best GW sources, are unknown or have ephemerides insufficiently precise to make a fully-coherent search tractable. Different search strategies are therefore used depending on available information.

CW searches are categorized as *all-sky* (for unknown objects), *directed* (sky location known) and *targeted* (spin frequency also known). When sky location and other ephemerides are known, computational cost can often be reduced or reinvested in increased sensitivity. As recently reviewed [17], directed [18, 19] and targeted [20, 21] searches now exist.

Signals from neutron stars with rotational periods of milliseconds should populate the GW spectrum. Millisecond pulsars appear to have a speed limit somewhat higher than 700 Hz but below their expected relativistic break-up speed [22]: GW emission is a possible cause. Dedicated analyses are motivated by the large fraction of these pulsars that are in binary systems.

Binary systems intrinsically have more parameters to analyze than isolated stars. TwoSpect [5] makes an all-sky search practical for unknown neutron stars in binary systems [6]. Other binary searches include developments of the Sideband [23, 24], Radiometer [25, 26], Polynomial [27], and CrossCorr [28, 29]. A systematic comparison [7] challenged these five methods to detect simulated signals from Sco X-1. A stacked  $\mathcal{F}$ -statistic search, derived from the coherent  $\mathcal{F}$ -statistic method [30], is under investigation [31].

Sco X-1 is an accreting Low Mass X-ray Binary (LMXB). LMXBs are believed to *spin-up* (increase rotational frequency) by accretion-driven recycling [32]. Accretion can also lead to non-axisymmetry that induces emission. These radiation mechanisms suggest a prime GW source. In the *torque balance* hypothesis, spin-up would continue until it equaled and canceled *spin-down* from GW emission [33]. This hypothesis can be quantified in terms of GW amplitude.

GW amplitude is characterized by the dimensionless strain amplitude  $h_0$ . The torque balance hypothesis predicts a strain  $h_0$  given by Equation 1. For an LMXB with flux  $\mathcal{F}_{\text{X-ray}}$  and NS that rotates at a frequency  $\nu_s$ , radiating at the quadrupolar GW radiation frequency  $f = 2\nu_s$  [34, 35],

$$h_0 \approx 4 \times 10^{-27} \left( \frac{300 \text{ Hz}}{\nu_s} \right)^{1/2} \left( \frac{\mathcal{F}_{\text{X-ray}}}{10^{-8} \text{ erg cm}^{-2} \text{ s}^{-1}} \right)^{1/2}. \quad (1)$$

With known X-ray flux but unknown frequency for Sco X-1, this limit can be evaluated for  $f$  between 50 and 1500 Hz [7], although large systematic uncertainties mean  $h_0$  could be larger or smaller:

$$h_0 \approx 3.5 \times 10^{-26} \left( \frac{600 \text{ Hz}}{f} \right)^{1/2},$$

$$\rightarrow h_0 < 2.2 \times 10^{-26} \text{ (} f = 1500 \text{ Hz)}, \quad h_0 < 1.2 \times 10^{-25} \text{ (} f = 50 \text{ Hz)}. \quad (2)$$

Torque balance hypothesizes that angular momentum from accretion counterbalances that lost to GW emission. If this is true,  $f$  remains relatively fixed for long durations, aside from spin-wandering due to variations in accretion. Computational costs are thus reduced by the restricted range of the frequency-derivative search. Accretion-driven GW emission strength would be a function of observed X-ray flux [34]. Higher X-ray emission implies higher GW strain amplitude. Lower torque balance frequency also implies higher amplitude.

The torque-balance levels predicted by Equation 2 are close to the estimated thresholds of detection of our searches, meriting effort in enhancing the sensitivity of our methods. TwoSpect directed search improvements skip the computation-saving hierarchical steps of the all-sky search, testing all points in parameter space with templates for enhanced sensitivity to a signal from a known sky location. This paper details the directed, fully-templated TwoSpect method and shows its application to simulated data containing Sco X-1 signals.

## 2. Signal model

GW signals are defined by  $h(t)$ , strain as a function of time. Models of  $h(t)$  in a binary search [5] depend on phase evolution,  $\Phi(t)$ ,

$$\Phi(t) = \Phi_0 + 2\pi f_0 \cdot \tau(t) + \Delta f_{\text{obs}} \cdot P \cdot \sin(\Omega[t - T_{\text{asc}}]), \quad (3)$$

$$h(t) = h_0 F_+ \frac{1 + \cos^2 \iota}{2} \cos \Phi(t) + h_0 F_\times \cos \iota \sin \Phi(t). \quad (4)$$

Here solar-system barycentered time is  $\tau(t)$  and  $\Phi(t = 0) \equiv \Phi_0$ . We also neglect spin-wandering, which could manifest as stochastic variation in  $\Phi_0$ .

The model does not currently search over *amplitude parameters*:  $h_0$  is the GW strain amplitude,  $\iota$  is the inclination angle of the neutron star with respect to the source,  $\psi$  is the GW polarization angle. While  $h_0$  can be recovered, its estimation is confounded by  $\iota$ . Both  $\iota$  and  $\psi$  affect amplitude through detector response, which depends on angle via the plus- and cross antenna functions,  $F_+$  and  $F_\times$ . Initial gravitational-wave phase,  $\Phi_0$ , further specifies the signal, but is neither searched nor recoverable with TwoSpect.

Our search is over unknown *Doppler parameters*, which drive signal evolution. Sky location  $(\alpha, \delta)$  is known for Sco X-1, as is orbital period  $P = 2\pi/\Omega$ . Initial orbital phase is fixed by time of ascension  $T_{\text{asc}}$ , to which TwoSpect is currently insensitive. Frequency  $f$  and projected semi-major axis  $a \sin i$  (expressed in light-seconds, ls) must be searched

over. Because the signal is frequency-modulated by the orbital motion of the source in the circular binary system, the latter parameter manifests through modulation depth  $\Delta f_{\text{obs}} = 2\pi f_0 \cdot (a \sin i)/(cP)$ .

### 3. TwoSpect analyses

The TwoSpect program is already described in detail [5, 6]. Only a brief summary is given here.

Data is read from a sequence of short Fourier transforms (SFTs), shorter than the total observation time  $T_{\text{obs}}$ . Noise and antenna pattern weights are applied to enhance the sensitivity of the search by weighting those SFTs that are more sensitive to a putative source. Each SFT contains  $K$  frequency bins. The Earth’s motion Doppler shifts the apparent frequency of a source, so these bins must be barycentered: their indices are shifted such that an unmodulated frequency from a given sky location remains in the same bin for all SFTs. These frequency bins represent the instantaneous frequency  $f$  of the signal. A second Fourier transform is performed, transforming the power in each frequency bin: the transform is from SFT time to  $f'$ . Effectively,  $f'$  represents the orbital frequency of the binary system.

TwoSpect templates are the  $M$  pixel weights  $w_i$  in the 2-D image-plane  $(f, f')$ . Each template corresponds to a signal model from the  $(f_0, \Delta f_{\text{obs}})$  astrophysical parameter space. After the second Fourier transform, the powers  $Z_i$  of data pixels in the  $(f, f')$  are measured and noise-background  $\lambda_i$  estimated. The test statistic,  $R$ , is the projection of the data (noise-subtracted powers) onto the templates, normalized by the templates:

$$R = \frac{\sum_{i=0}^{M-1} w_i [Z_i - \lambda_i]}{\sum_{i=0}^{M-1} [w_i]^2}. \quad (5)$$

Estimated  $p$ -values for this statistic allow determination of detection probability. Expositions of the TwoSpect detection statistic and signal model can be found in previous methods papers [5, 36].

## 4. Application to directed searches

### 4.1. Sensitivity and computational cost

The original design of the all-sky TwoSpect analysis employs a hierarchical analysis scheme to control computational costs while still maintaining good sensitivity to a broad parameter space [5]. Each narrow frequency band requires corrections for the Doppler effect caused by Earth’s motion. Because this correction depends on sky position, an all-sky search for typical SFT lengths of several minutes would need  $\mathcal{O}(10^{18})$  templates; in practice, an incoherent harmonic sum is used to reduce this number, but it also limits sensitivity [5]. Directed searches can use  $\mathcal{O}(10^8)$  templates at a single sky location with full sensitivity, because  $R$ -statistics are returned for every template.

**Table 1.** Scorpius X-1 prior measured parameters from electromagnetic observations. Note that the projected semi-major axis value is derived from a velocity amplitude of  $K_1 = 40 \pm 5 \text{ km s}^{-1}$  [7, 30].

Sco X-1 parameter	Value	Units
Distance [39]	$2.8 \pm 0.3$	kpc
Eccentricity ( $\epsilon$ ) [7]	$< 0.068 (3\sigma)$	—
Right ascension ( $\alpha$ ) [40]	$16:19:55.067 \pm 0.06''$	—
Declination ( $\delta$ ) [40]	$-15^\circ 38' 25.02'' \pm 0.06''$	—
X-ray flux at Earth ( $\mathcal{F}_{\text{X-ray}}$ ) [35]	$3.9 \times 10^{-10}$	$\text{W m}^{-2}$
Orbital period ( $P$ ) [37]	$68023.70 \pm 0.04$	s
Projected semi-major axis ( $a \sin i$ ) [41]	$1.44 \pm 0.18$	ls

For Sco X-1, distance, eccentricity, X-ray luminosity, sky location, and orbital period are known with good precision and projected semi-major axis is measured to be  $1.44 \pm 0.18$  ls, (Table 1). NS spin frequency, however, is unknown [37]. Other targets for TwoSpect, such as XTE J1751-305 [38], have known frequency, reducing computational costs substantially further.

A directed search over projected semi-major axis in the range  $[-3\sigma_{a \sin i}, +3\sigma_{a \sin i}]$ , around the measured value, and over GW signal frequency  $f$  from  $f_{\min}$  to  $f_{\max}$ , incurs a predictable computational cost. With a fixed rectangular parameter spacing of  $1/(2T_{\text{coh}})$  in  $f$  and  $1/(4T_{\text{coh}})$  in  $\Delta f_{\text{obs}}$ , using SFTs of coherence time  $T_{\text{coh}}$  and analysis bands of width  $f_{\text{bw}}$ , the search uses  $N_{\text{template}}$  templates per interferometer:

$$N_{\text{template}} = [1 + 2f_{\text{bw}}T_{\text{coh}}] \times \sum_{j=1}^{j=\frac{f_{\max}-f_{\min}}{f_{\text{bw}}}} \left[ 1 + 2\pi (f_{\min} + jf_{\text{bw}}) \frac{4T_{\text{coh}}}{P} 6\sigma_{a \sin i} \right], \quad (6a)$$

$$= 2 \left( T_{\text{coh}} + \frac{1}{f_{\text{bw}}} \right) \left[ 1 + \frac{4\pi T_{\text{coh}}}{P} (6\sigma_{a \sin i})(f_{\max} + f_{\min} + f_{\text{bw}}) \right] (f_{\max} - f_{\min}). \quad (6b)$$

#### 4.2. Participation in a Sco X-1 mock data challenge

Several analyses are applicable to a search for continuous GW from known neutron stars in binary systems. TwoSpect is capable of searching for unknown systems<sup>‡</sup>. The Scorpius X-1 Mock Data Challenge (MDC) compares five methods [7]. This MDC simulates 50 *open*, unblinded and 50 *closed*, blinded signals, with signal parameters drawn from Sco X-1 astrophysical priors. Each signal is also known as an *injection*. Three interferometers are simulated: H1 (Hanford), L1 (Livingston), and V1 (Virgo). Within 100 frequency bands of 5 Hz each,  $f$  is uniformly distributed. Bands cover a range from 50 to 1500 Hz and contain Gaussian noise simulating a detector with noise floor  $4 \times 10^{-24} \text{ Hz}^{-1/2}$ , the expected Advanced LIGO minimum. Projected semi-major axis  $a \sin i$  is Gaussian distributed with mean 1.44 ls and standard deviation 0.18 ls. Period  $P$  is Gaussian distributed with mean 68023.70 s and standard deviation 0.04 s.

<sup>‡</sup> Other all-sky binary search programs are based on the Polynomial [27] and Radiometer [26] methods.

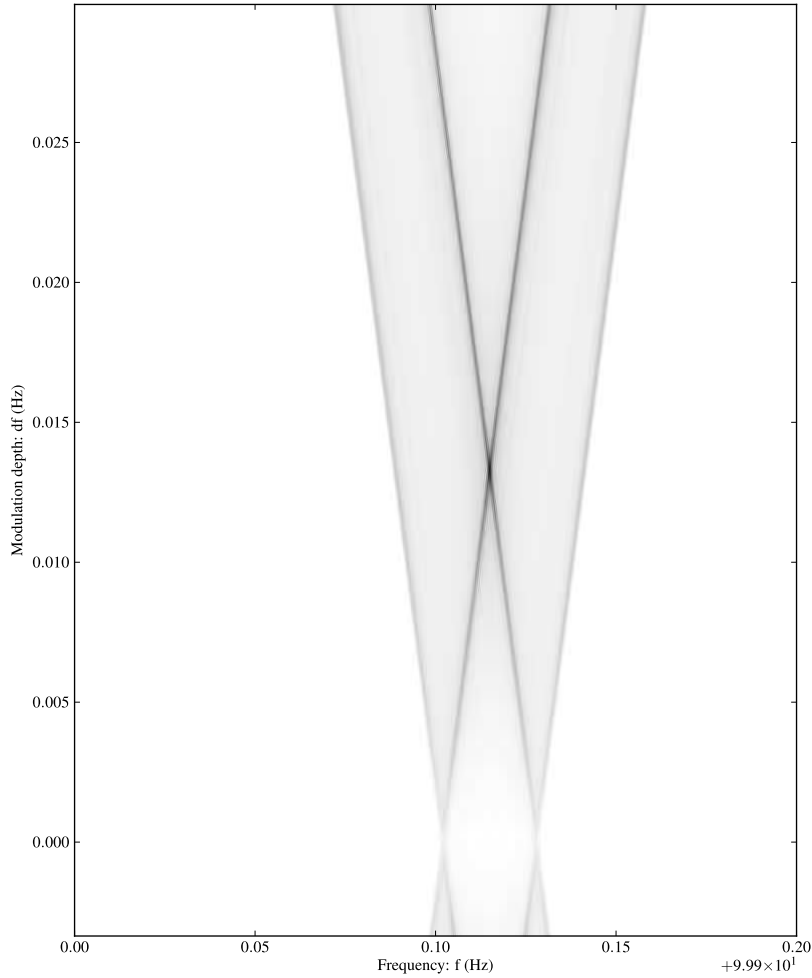


**Figure 1.** Simulated signal, 100.015 Hz frequency ( $f$ ), 1.44 ls projected semi-major axis (modulation depth 0.0133 Hz,  $\Delta f_{\text{obs}}$ ), showing single-template  $-\log_{10} p$ -value. The graph spans 241 templates in  $\Delta f_{\text{obs}}$ , 721 in  $f$ , twice as dense in  $\Delta f_{\text{obs}}$  as in  $f$ . A signal with  $h_0 = 4 \times 10^{-21}$  is injected into a Gaussian noise amplitude spectral density of  $4 \times 10^{-24} \text{ Hz}^{-1/2}$ , observed for  $10^6$  seconds. The  $p$ -value is extrapolated from the  $R$  statistic. For illustration,  $\Delta f_{\text{obs}}$  extends below zero to show that the code is well-behaved and that the algorithm gracefully mirrors results for negative input parameters. Most importantly,  $-\log_{10} p$  is maximal at the true parameters. Signal is partly recovered when template  $f$  differs from the true signal by plus or minus  $\Delta f_{\text{obs}}$ , and also when template  $f$  and  $\Delta f_{\text{obs}}$  differ equally from the true parameters.

Sky location is  $(\alpha, \delta) = (16:19:55.067, -15^\circ 38' 25.02'')$ . The uncertainty in period is small enough that it is not a free parameter in the directed search using the TwoSpect pipeline. TwoSpect conducts a search in  $f$  and  $a \sin i$  for a fixed period, requiring approximately  $N_{\text{template}} = 5.0 \times 10^7$  templates per interferometer, covering 100 bands of 5 Hz each, 500 Hz total. With three interferometers,  $1.5 \times 10^8$  templates are searched.

Figure 1 shows a wide analysis that is magnified in Figure 2. These analyses require minimal modification from that of the all-sky search:  $R$ -statistic and  $p$ -value code was identical, aside from looping over all template positions in the parameter grid.

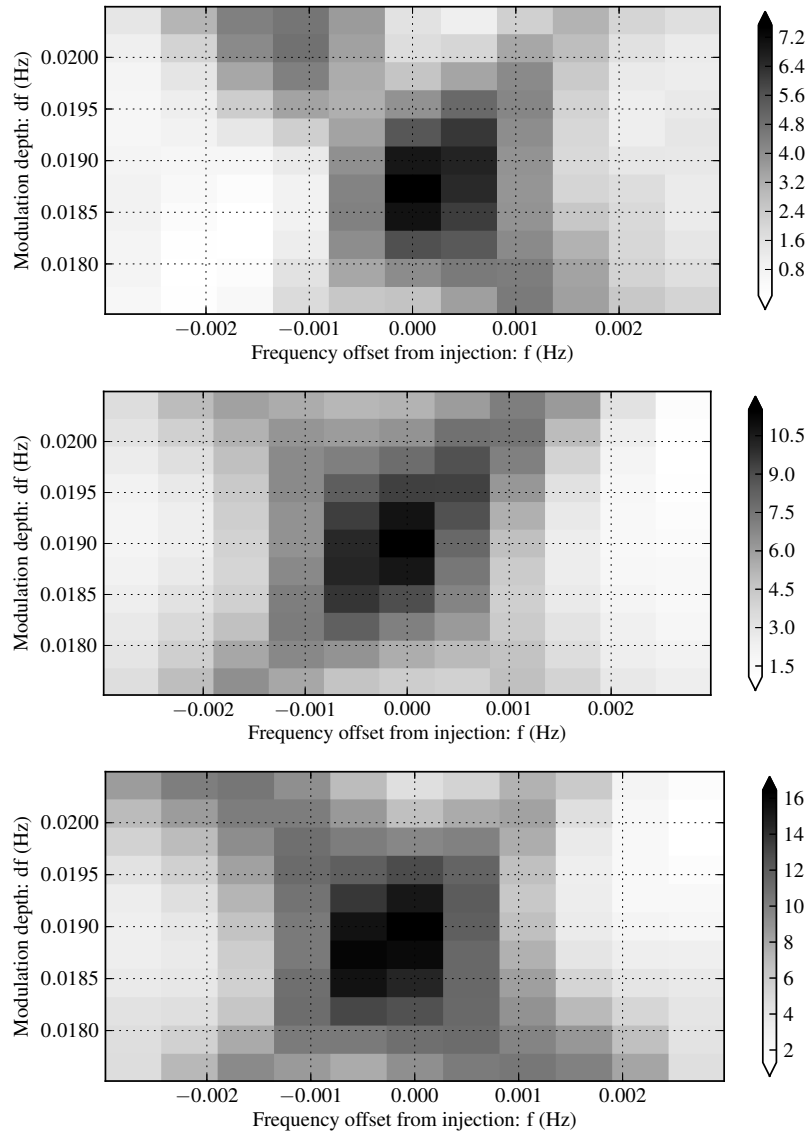


**Figure 2.** Heatmaps for H1, L1, and V1 detectors (top to bottom), of  $-\log_{10} p$ -value for 11x11 templates centered on Sco X-1 MDC signal 8. This injection was detectable in a year of simulated data at  $h_0 = 5.6 \times 10^{-25}$  in noise of  $4 \times 10^{-24} \text{ Hz}^{-1/2}$  and  $\cos \iota = 0.09$ . Maxima for all detectors are within a template of the true parameters.

## 5. Directed search demonstration and outlier follow-up

Directed TwoSpect search methods can be demonstrated through the mock data challenge described in Section 4. Post-processing is the main modification required for the pipeline in the directed search: new detection criteria and techniques for parameter and upper limit estimation are required, because the fully-templated output differs significantly from that of hierarchical search.

### 5.1. Overview of detection and parameter estimation

A set of extremal  $p$ -value outliers in 5 Hz bands is produced for each interferometer, subject to a  $p$ -value threshold inferred from Gaussian noise. These sets are compared in pairwise coincidence between interferometers (H1-L1, H1-V1, or L1-V1). Coincidence of outliers allows  $f$  or  $\Delta f_{\text{obs}}$  to differ by  $\leq 1/T_{\text{coh}}$  between interferometers, based on prior experience from the all-sky search [6]. This allowed difference is 2 steps in the  $f$  grid or 4 in the  $\Delta f_{\text{obs}}$  grid. Surviving outliers are classified as detections.

For a given detection in one band, the signal parameters are inferred from the values of the template with the highest (single-interferometer)  $p$ -value. These parameters include  $f$ ,  $a \sin i$ , and  $h_0$ . Again, for open signals, the true parameters were known in advance. Total uncertainty in  $f$  and  $a \sin i$ , and non-systematic uncertainty (random) in  $h_0$ , is determined from the standard deviation of the set of parameters of recovered open signals compared to their true parameters, as detailed in section 5.3.

The estimated strain is  $h_{\text{rec}} \propto R^{1/4}$ . Systematic uncertainty arises from the unknown inclination angle,  $\cos \iota$ , which dominates the total uncertainty in strain. This ambiguity cannot be resolved with the present algorithm and depends partially on the assumed prior distribution of signal amplitudes; the uncertainty is estimated by simulation in Section 5.4. With new algorithm enhancements,  $\cos \iota$  can become a search parameter.

Due to the uniform noise floor and low number of injections, a single upper limit value is declared for all 100 bands based on the best estimate of the 95% confidence level of non-detected signals in the open set of injections.

### 5.2. Detection claims

Studying the Gaussian noise in the Scorpius X-1 MDC open data set, we can set thresholds for detection.

To obtain a Gaussian noise sample, we excise injection signals, which are visible in the  $f$  vs  $\Delta f_{\text{obs}}$  plane. The excised region depends on injection frequency  $f_{\text{inj}}$  and modulation depth  $\Delta f_{\text{inj}}$ , on the Earth-orbital Doppler shift ( $\approx 10^{-4}$ ), and additional bins (at least 10) to avoid spectral leakage. The half-width excised for each injection is  $\delta f_{\text{inj}}$ :

$$\delta f_{\text{inj}} = 2 \times (10^{-4} \times f_{\text{inj}} + \Delta f_{\text{inj}}) + \frac{10}{360} \text{Hz}. \quad (7)$$

The remaining noise sample is the data set with all intervals  $[f_{\text{inj}} - \delta f_{\text{inj}}, f_{\text{inj}} + \delta f_{\text{inj}}]$  removed. In the remaining noise sample, the estimated  $p$ -value distribution is not perfectly uniform, due to gaps in the data. Nonetheless, the noise sample provides a distribution of template  $R$ -statistics and  $p$ -values in the absence of signals. This procedure provides an empirical measure of the estimated  $p$ -value that corresponds to an actual false alarm probability of 1% per 5 Hz frequency band. Taken together, these let us establish detection criteria.

If there is any candidate surviving the following criteria in a 5 Hz band, we mark it detected, else not detected:

- single-IFO candidates are the top 200 most extreme  $p$ -value outliers in a 5-Hz band, of those that pass a  $\log_{10} p \leq \mathcal{T}$  threshold, where  $\mathcal{T} = -7.75$  if  $f < 360.0$  Hz (those that used 840-s SFTs) or  $-12.0$  if  $f \geq 360.0$  Hz (those that used 360-s SFTs). Note: The large discrepancy between the  $p$ -value thresholds in the MDC is a historical artifact from a configuration error. The discrepancy is much reduced when this is fixed, as done for future analyses. Our expectation remains that the threshold should be independent of coherence time.
- each candidate must survive at least one double-IFO coincidence test, involving a pairwise comparison of single-IFO candidates to see whether they are within  $1/T_{\text{SFT}}$  in both frequency ( $f$ ) and modulation depth ( $\Delta f_{\text{obs}}$ ).

### 5.3. Parameter estimation and uncertainty for detected signals

The open set of signals, of which 31 of 50 were detected, are the foundation for TwoSpect's parameter estimates. The reconstructed  $h_0$  output from TwoSpect is  $h_{\text{rec}} = CR^{1/4}$ . The value of  $C$  is determined from the mean value of a large number of simulations for circularly-polarized waves over the whole sky and full range of  $f$ ,  $P$ , and  $\Delta f_{\text{obs}}$ .

Then  $h_{\text{rec}}$  is rescaled twice, first by  $\rho_R$  for more accurate measurement at the Sco X-1 period and modulation depth, and second by  $\rho_{\cos \iota}$  for unknown  $\cos \iota$ . Thus the final claimed value of  $h_0$  for a signal  $j$  is  $(h_0)_j$ :

$$(h_0)_j = \rho_R \rho_{\cos \iota} h_{\text{rec},j}. \quad (8)$$

The first scale factor,  $\rho_R = 1.11$ , corrects the average values of  $h_{\text{rec}}$  ( $h_0$ -reconstructed) in the open set to match the corresponding  $h_{\text{eff}}$  ( $h_0$ -effective, given circular polarization weightings). That is,  $\bar{h}_{\text{eff}} = 1.11 \times \bar{h}_{\text{rec}}$ , where  $h_{\text{eff}}$  is defined *a priori* by  $h_{\text{inj}}$  ( $h_0$ -injected) and  $\cos \iota$ :

$$h_{\text{eff}} = \frac{1}{\sqrt{2}} \sqrt{\left(\frac{1 + \cos^2 \iota}{2}\right)^2 + (\cos \iota)^2} \times h_{\text{inj}}. \quad (9)$$

In the MDC study [7], 4 of the 31 detected, open signals account for the largest frequency estimation error. This error arose from a misconfiguration that does not affect the other analyses; it was addressed by taking those 4 as one class and the remaining 27 as another, a step that should be unnecessary in future analyses. Then, the uncertainty due to random error for  $h_0$ ,  $f$ , and  $a \sin i$  is estimated by the standard deviation between the recovered and true parameters:

$$\sigma_f^2 = \frac{1}{N_{\text{open}} - 1} \sum_{j \in \{\text{open}\}}^{N_{\text{open}}} (f_{\text{rec},j} - f_{\text{inj},j})^2, \quad (10)$$

$$\sigma_{a \sin i}^2 = \frac{1}{N_{\text{open}} - 1} \sum_{j \in \{\text{open}\}}^{N_{\text{open}}} ((a \sin i)_{\text{rec},j} - (a \sin i)_{\text{inj},j})^2, \quad (11)$$

$$\sigma_{h_0, \text{rand}}^2 = \frac{1}{N_{\text{open}} - 1} \sum_{j \in \{\text{open}\}}^{N_{\text{open}}} (\rho_R \times h_{\text{rec},j} - h_{\text{eff},j})^2, \quad (12)$$

where  $N_{\text{open}}$  is the number of open injections,  $\sigma_f$ ,  $\sigma_{a \sin i}$ , and  $\sigma_{h_0}$  are the uncertainties we state for recovered  $f_{\text{rec}}$ ,  $(a \sin i)_{\text{rec}}$ , and  $h_{\text{rec}}$  given injected  $f_{\text{inj}}$ ,  $(a \sin i)_{\text{inj}}$ , and  $h_{\text{inj}}$ .

The error between injected and recovered parameters does not show any other clear correlation with  $p$ -value or signal frequency, at least in the 31 detected signals. Except for the most marginally detected signals, where noise fluctuations matter, uncertainty in  $f$  and  $a \sin i$  is dominated by the template grid spacing. The  $\sigma_f$  and  $\sigma_{a \sin i}$  error bars are used uniformly for claiming uncertainties on the signals in the MDC.

The largest source of uncertainty for  $h_0$  comes from corection for systematic underestimation, multiplying a factor of 1.74 into  $C$ . This uncertainty is the ambiguity in  $\cos \iota$  discussed in Section 5.4. Parameter estimation uncertainty for  $f$  and  $a \sin i$  is then just the random error; for  $h_0$ , it is the quadrature sum of random error and  $\cos \iota$  ambiguity.

#### 5.4. Ambiguity from $\cos \iota$

The largest systematic uncertainty in  $h_0$  comes from the unknown  $\cos \iota$ . TwoSpect is optimized for  $|\cos \iota| = 1$  and computes the  $R$  statistic by weighting the SFTs assuming circularly-polarized GWs, which still provides good sensitivity for other polarizations. Recall that  $h_{\text{rec}}$  must be scaled by  $\rho_R = 1.11$  to match  $h_{\text{eff}}$ . When a source is circularly-polarized, TwoSpect estimates  $\rho_R h_{\text{rec}} \approx h_{\text{inj}}$ . In the case of linear polarization, Equation 9 indicates that  $h_{\text{inj}}$  will be about  $2^{3/2}$  times larger than  $h_{\text{eff}}$  (and so  $h_{\text{rec}}$ ). The aim is to find an average conversion factor from  $h_{\text{rec}}$  to  $h_{\text{inj}}$  and a robust estimate of the uncertainty.

Since  $h_{\text{eff}}$  of circularly-polarized signals is greater, those signals are more easily detectable than linearly-polarized signals of equivalent  $h_{\text{inj}}$ . Therefore the signals that are detectable are biased, near threshold, to being more likely circularly-polarized. This “circularizes” the correction factor, depending on the detection efficiency of the pipeline and on the assumed prior distribution of strain amplitudes. Although the effect is minor, estimating its size requires simulation.

The simulation generates 2 million signal amplitudes between  $h_{\text{inj}} = 3 \times 10^{-26}$  and  $h_{\text{inj}} = 3 \times 10^{-24}$  with a distribution of  $1/h_0$ , the assumed prior distribution of  $h_0$  values. This simulation code is independent of TwoSpect. In this simulation,  $\rho_R$  is 1 for simplicity, so we can treat  $h_{\text{rec}} = h_{\text{eff}}$  here. We model detection efficiency by assuming no signals are detected below  $h_{\text{eff}} = 1 \times 10^{-25}$ , all are detected above  $h_{\text{eff}} = 3 \times 10^{-25}$ , and the fraction detected is linear in  $h_0$  between those values. Together with a uniform  $\cos \iota$  distribution of  $[-1, 1]$ , this leads to a trapezoidal distribution of recovered, detected  $h_0$  values with a curved lower (left) edge (Figure 3).

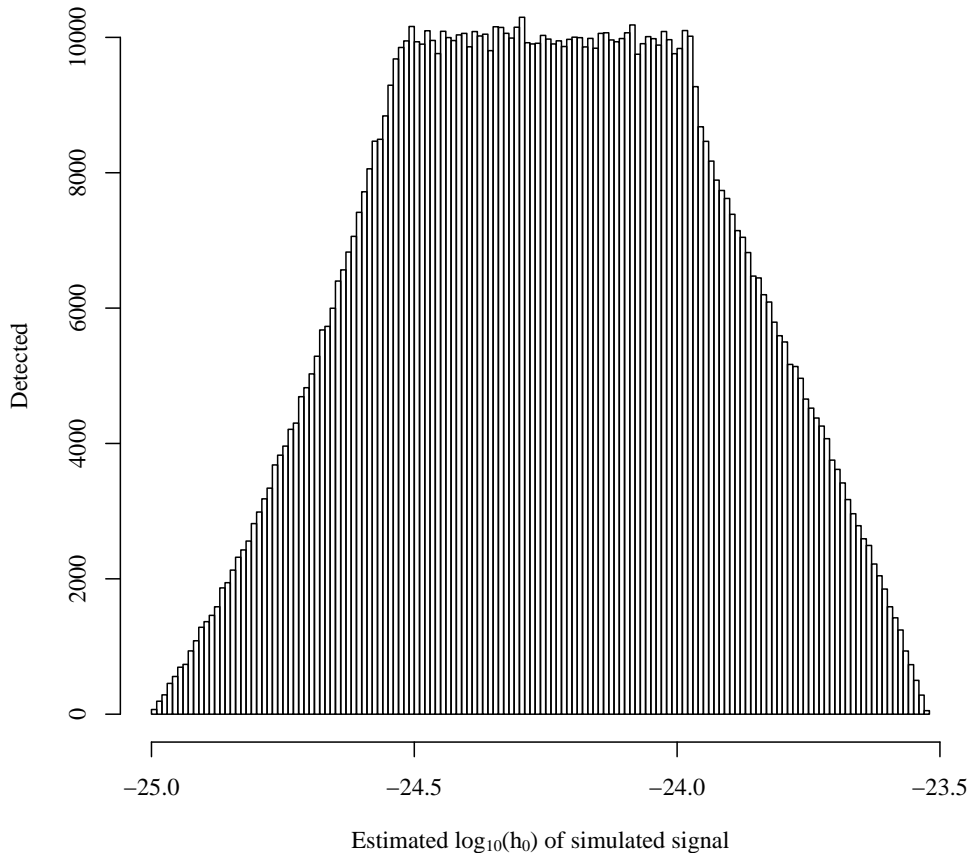


**Figure 3.** Histogram, 150 bins, of the distribution of 2 million simulated signals, strain between  $3 \times 10^{-26}$  and  $3 \times 10^{-24}$  under a log-uniform distribution, following application of  $\cos \iota$  and detection efficiency cuts.

Part of the domain of the simulation must be excluded. To find the average  $h_{\text{inj}}/h_{\text{rec}}$  for a given  $h_{\text{rec}}$ , every  $h_{\text{rec}}$  must correspond to a full sampling of the range of polarizations. A large  $h_{\text{inj}}$  with linear polarization or small  $h_{\text{inj}}$  with circular polarization could have the same  $h_{\text{rec}}$ . No linearly-polarized signals could produce  $h_{\text{rec}}$  above  $1 \times 10^{-24}$ , because Equation 9 shows that the largest signal,  $h_{\text{inj}} = 3 \times 10^{-24}$ , would be reconstructed a factor of  $2\sqrt{2}$  smaller, at  $h_{\text{rec}} = 1.06 \times 10^{-24}$  (again,  $\rho_R = 1$  for the simulation). Above  $1 \times 10^{-24}$ , polarizations tend to be more circular, thus the average ratio must exclude this region or it will be biased by the limited range of the simulation  $h_{\text{inj}}$ . Expanding the domain would raise the cutoff, although the resulting ratio would no longer perfectly correspond to the MDC.

With the domain of the simulation determined, we compute that mean ratio of  $h_{\text{inj}}$  to  $h_{\text{rec}}$  to be 1.74. Fine-binning  $h_{\text{rec}}$ , an interval of  $[1.74 - \sigma_{\cos \iota}, 1.74 + \sigma_{\cos \iota}]$  encloses 68% of corresponding  $h_{\text{inj}}$  when  $\sigma_{\cos \iota}$  is 0.37 (found by manual optimization). Therefore our best estimate for the correction factor  $\rho_{\cos \iota}$ , with  $\sigma_{\cos \iota}$  inferred as the standard deviation, is  $1.74 \pm 0.37$ . This factor multiplies  $\rho_R$ , which is 1.11 in the actual search.

The systematic uncertainty, being the uncertainty  $\sigma_{\cos \iota}$  in the correction factor, scales with signal strength; the non-systematic (random) is fixed and is also multiplied

by the correction factor. The final estimate of the uncertainty in  $h_0$  for signal  $j$  is the quadrature sum of the systematic and non-systematic uncertainties:

$$\sigma_{(h_0),j} = \sqrt{(\rho_{\cos \iota} \times \sigma_{h_0,\text{rand}})^2 + (\sigma_{\cos \iota} \times \rho_R \times h_{\text{rec},j})^2}. \quad (13)$$

### 5.5. Accuracy of parameter estimation uncertainty claims

This scheme reliably recovers parameters to within the stated uncertainties, as shown in the MDC [7]. Verifying the calibration factors and confidence intervals once more, one can confirm that a conservative fraction of  $h_0$ ,  $f$  and  $a \sin i$  are within their  $1\text{-}\sigma$  error bars: 77.4% for  $\sigma_{h_0}$ , 74.2% for  $\sigma_f$ , and 67.7% for  $\sigma_{a \sin i}$ .

### 5.6. Upper limits for undetected signals and detection efficiency

Only upper limits have come from CW searches to date. Until GWs are detected from neutron stars, the scientific value of a CW analysis is to constrain the plausible  $h_0$  and inferred ellipticity from those stars. For the MDC-simulated signals, we use a simplified method to estimate upper-limits. In a real detector, noise varies with frequency [42]; in this simulation, the noise floor is flat at  $4 \times 10^{-24} \text{ Hz}^{-1/2}$ . In reality we would inject a large number of simulated signals into a number of smaller bands, in order to understand the upper limit as a function of frequency.

To measure detection efficiency, we calculate the  $h_{\text{eff}}$  for all signals and find the average detection rate for a given  $h_{\text{eff}}$ . Binomial uncertainty is also calculated and each  $1\text{-}\sigma$  deviation (per 5-signal bin) is graphed in Figure 4, which shows a least-squares sigmoid fit. This detection efficiency curve maps from strain to probability of detection. Next we would like an upper limit function that takes a probability as an input and returns a strain that, with the given probability, is no less than the actual strain.

To characterize the upper limit, we plot the distribution of  $h_{\text{rec}}$  versus injected  $h_{\text{eff}}$  in Figure 5. We verify that 95% of non-detected open signals are covered by a naive upper limit of  $h_{\text{rec}} = 2.19 \times 10^{-25}$ . This claim does not rely on binning but rather on the sampling density of the injections. This number, when corrected by the  $\rho_R$  rescaling factor of 1.11 and  $\cos \iota$  correction  $\rho_{\cos \iota}$  of 1.74, yields the upper limit of  $(1.74) \times (1.11) \times 2.19 \times 10^{-25} = 4.23 \times 10^{-25}$  for TwoSpect. Because of the flat noise floor, this is reported as a single upper limit for any non-detections in the MDC. Frequency-dependent methods are under development for actual observations.

## 6. Conclusions

### 6.1. MDC results

TwoSpect analyses applied to the MDC data set detect more stars than the Radiometer, Sideband, or Polynomial pipelines; only the CrossCorr algorithm found more signals [7]. Each detection includes an estimate of  $a \sin i$ , which is not produced by Radiometer, Sideband, or Polynomial. The MDC did not model the spin-wandering of the neutron

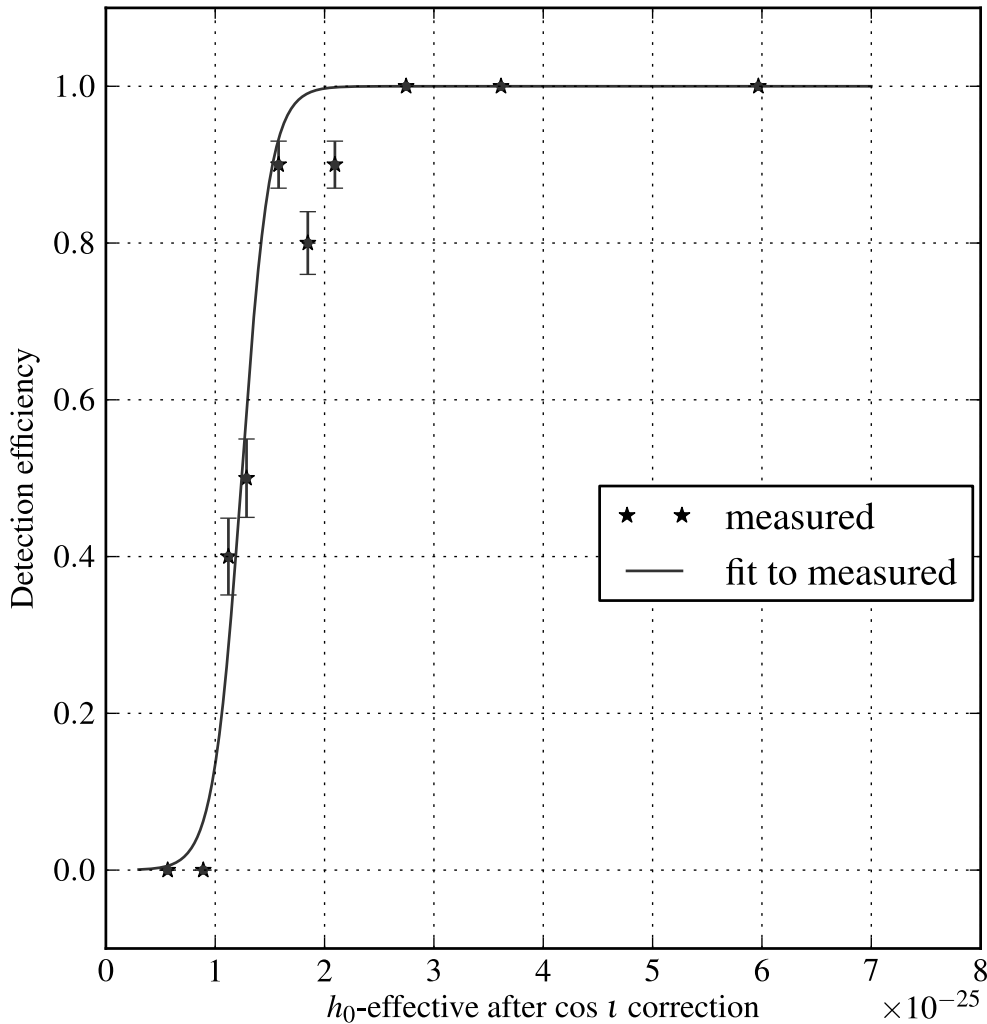


**Figure 4.** Detection efficiency for open and closed signals. Because only 100 signals are in the data set, this curve has fluctuations and large  $1\text{-}\sigma$  error bars. Moreover, the binomial error for these error bars is zero in bins where no or all signals are detected, which is not necessarily realistic. The 95% level is just below  $2 \times 10^{-25}$  (before rescaling factors of 1.74 and 1.11), corroborating better methods of estimating the upper limit.

star that is expected in real data, although participants were told to assume its presence, and spin-wandering is planned for future MDCs. Spin-wandering is an effect to which TwoSpect is theoretically highly robust. TwoSpect has already been applied to real data [6], though not using the directed search, in a fully-templated mode. This experience with real data remains the strongest argument for the method’s capabilities. In all, 34 of 50 closed (and 31 of 50 open) signals are detected, and  $f$ ,  $a \sin i$ , and  $h_0$  are estimated. Strain upper limits of  $4.23 \times 10^{-25}$  noise of in  $4 \times 10^{-24}$  strain  $\text{Hz}^{1/2}$  are determined for the 16 non-detected, closed signals. Although the distribution of  $h_0$  values in the MDC was astrophysically optimistic, the MDC validated our ability to claim detections and recover orbital and GW parameters accurately.

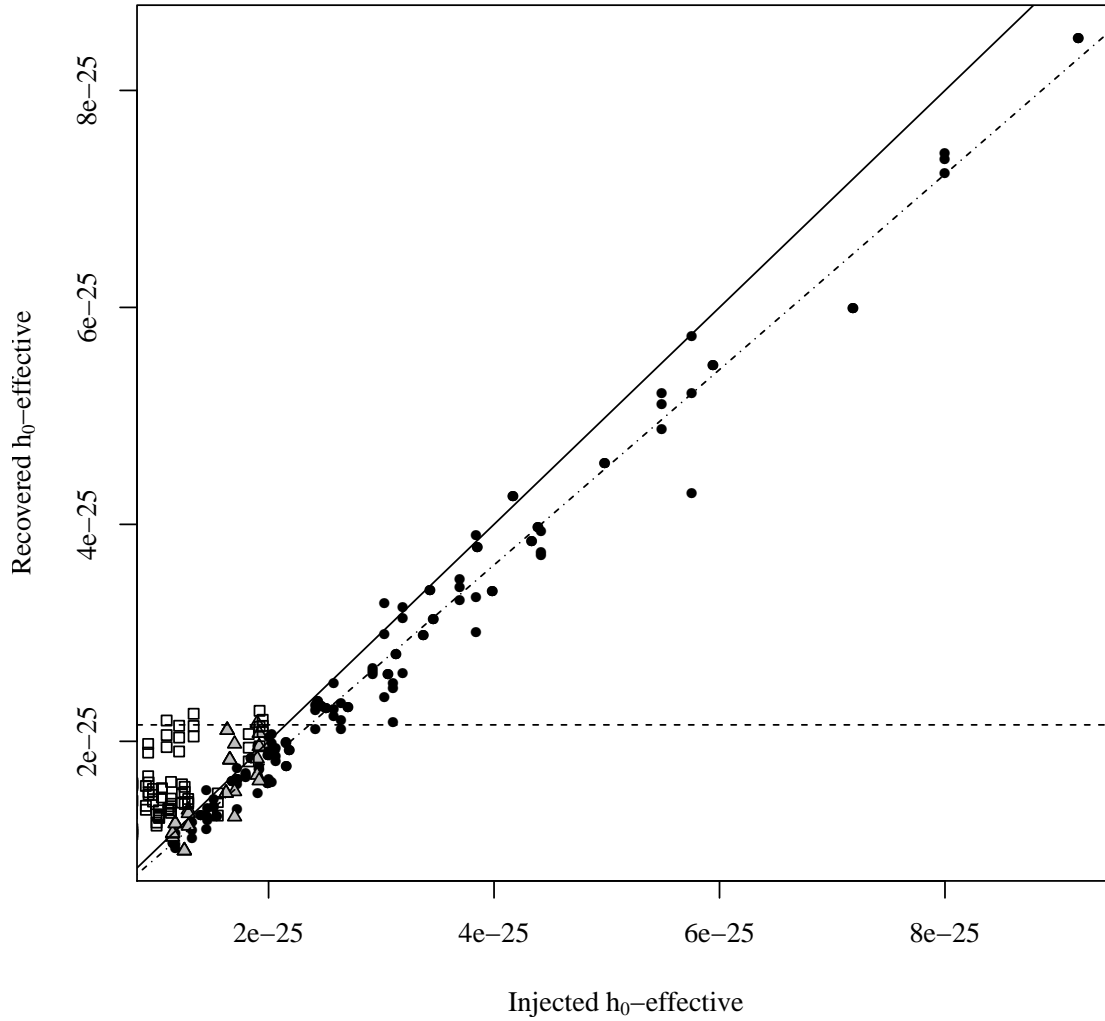


**Figure 5.** Detections and upper limit determination, with all 100 simulated signals. Injections are seen in three (black circle), one (gray triangle), or zero (open box) detector pairs and plotted in recovered strain versus effective circular strain injected. The most significant template is shown, in each band, in each interferometer, whether detected or not. (There are no injections seen with two detection pairs, because this plot shows only the loudest outlier from each 5 Hz band; if some injection were seen in two and not three pairs, it would mean two distinct coincidences were seen, only one of which would be the loudest). We identify a shelf of non-detected signals that are 95% covered by an upper limit about  $2.19 \times 10^{-25}$ . This number, when corrected, yielded the upper limit of  $1.74 \cdot 1.11 \cdot 2.19 \times 10^{-25} = 4.23 \times 10^{-25}$  for TwoSpect. The unity-slope black line is shown to ascertain whether a further empirical rescaling factor is needed to match the dashed-and-dotted least-squares linear fit (it is: constant 1.11). The zero-slope horizontal dashed line is shown to indicate the ninety-five percent confidence upper limit in the absence of detection.

### 6.2. Future directed binary searches for continuous GWs

Algorithms such as TwoSpect are designed so an astrophysically-plausible strain from Sco X-1, believed from torque-balance arguments to be around  $10^{-25}$  might be found. The previously-published TwoSpect all-sky search in a year of S6 data set an exemplary upper limit of  $2.3 \times 10^{-24}$  in noise with a strain amplitude spectral density of  $2 \times 10^{-23} \text{ Hz}^{-1/2}$ . Extrapolating to Advanced LIGO design sensitivities of  $4 \times 10^{-24} \text{ Hz}^{-1/2}$ , this implies a strain around  $4.6 \times 10^{-25}$ . The directed search method demonstrated in this paper achieved an  $4.23 \times 10^{-25}$  upper limit in equivalent simulated data, a comparable sensitivity depth (factor below the noise floor [43]). While real data complications may worsen this limit, several simplified and conservative steps were taken, and the limit should overall improve when fully tested with injections as in the all-sky search. Additional improvements to the algorithm, such as coherent SFT summing, have been developed [36] and could further improve this limit in the future.

Comprehensively covering the parameter space of Sco X-1 at full sensitivity with the directed search, instead of hierarchically as in the previous search, increases the probability of detection. When detections do occur, the ability of TwoSpect to determine the frequency and projected semi-major axis of the neutron star in the binary system will prove highly informative. Analyses of real data for signals from Scorpius X-1 and additional neutron stars in binary systems, such as XTE J1751-305, are underway. In the long term, we hope that the discovery of gravitational waves from neutron stars in LMXBs will provide a firm link between our observations and electromagnetic astronomy.

### Acknowledgments

This work was partly funded by National Science Foundation grants NSF PHY 1205173 and NSF PHY 1505932. These investigations have taken place as part of the LIGO Scientific Collaboration. The Mock Data Challenge for Scorpius X-1 was organized by Chris Messenger. Thanks to Maria Alessandra Papa for providing extensive guidance and support. Code for this paper is available online [44]. This document bears LIGO DCC number P1500037.

### References

- [1] Manchester R, Hobbs G, Teoh A and Hobbs M 2005 *Astronom. J.* **129** 4
- [2] Harry G *et al.* 2010 *Class. Quant. Grav.* **27** 084006
- [3] Acernese F *et al.* 2009 Advanced Virgo baseline design Tech. Rep. VIR-0027A-09 Virgo
- [4] Goetz E A 2010 *Gravitational wave studies: detector calibration and an all-sky search for spinning neutron stars in binary systems* Ph.D. thesis University of Michigan

- [5] Goetz E and Riles K 2011 *Class. Quant. Grav.* **28** 215006
- [6] Aasi J *et al.* 2014 *Phys. Rev. D* **90** 062010
- [7] Messenger C, Bulten H J, Crowder S G, Dergachev V, Galloway D K, Goetz E, Jonker R J G, Lasky P D, Meadors G D, Melatos A, Premachandra S, Riles K, Sammut L, Thrane E H, Whelan J T and Zhang Y 2015 *Phys. Rev. D* **92**(2) 023006
- [8] Brady P, Creighton T, Cutler C and Schutz B 1998 *Phys. Rev. D* **57**(4) 2101
- [9] Shawhan P 2010 *Class. Quant. Grav.* **27** 084017
- [10] Owen B 2010 *Phys. Rev. D* **82** 104002
- [11] Jaranowski P, Królak A and Schutz B 1998 *Phys. Rev. D* **58** 063001
- [12] Krishnan B, Sintès A M, Papa M A, Schutz B F, Frasca S and Palomba C 2004 *Phys. Rev. D* **70** 082001
- [13] Abbott B 2008 *Phys. Rev. D* **77** 022001
- [14] Abbott B *et al.* 2009 *Phys. Rev. Lett* **102** 111102
- [15] Dergachev V 2010 *Class. Quant. Grav.* **27** 205017
- [16] Abadie J *et al.* 2012 *Phys. Rev. D* **85** 022001
- [17] Riles K 2013 *Prog. in Particle & Nucl. Phys.* **68** 1
- [18] Wette K *et al.* 2008 *Class. Quant. Grav.* **25** 235011
- [19] Abadie J *et al.* 2010 *ApJ* **722** 1504
- [20] Dupuis R and Woan G 2005 *Phys. Rev. D* **72** 102002
- [21] Aasi J *et al.* 2014 *Astrophys. J* **785** 119
- [22] Chakrabarty D *et al.* 2003 *Nature* **424** 42
- [23] Messenger C and Woan G 2007 *Classical and Quantum Gravity* **24** S469
- [24] Sammut L, Messenger C, Melatos A and Owen B 2014 *Phys. Rev. D* **89** 043001
- [25] Ballmer S W 2006 *Classical and Quantum Gravity* **23** S179
- [26] Abadie J *et al.* 2011 *Phys. Rev. Lett.* **107** 271102
- [27] van der Putten S, Bulten H J, van den Brand J F J and Holtrop M 2010 *Journal of Physics Conference Series* **228** 012005
- [28] Dhurandhar S, Krishnan B, Mukhopadhyay H and Whelan J T 2008 *Phys. Rev. D* **77**(8) 082001
- [29] Whelan J T, Sundaesan S, Zhang Y and Peiris P 2015 *Phys. Rev. D* **91**(10) 102005
- [30] Abbott B *et al.* 2007 *Phys. Rev. D* **76** 082001
- [31] Leaci P and Prix R 2015 *Phys. Rev. D* **91**(10) 102003
- [32] Papaloizou J and Pringle J 1978 *MNRAS* **184** 501
- [33] Wagoner R 1984 *Ap. J.* **278** 345
- [34] Bildsten L 1998 *Astrophys. J. Lett.* **501** L89
- [35] Watts A, Krishnan B, Bildsten L and Schutz B 2008 *MNRAS* **389** 839

- [36] Goetz E and Riles K 2015 *LIGO DCC* **P1500038**
- [37] Galloway D K, Premachandra S, Steeghs D, Marsh T, Casares J and Cornelisse R 2014 *Ap J* **781** 14 (*Preprint* 1311.6246)
- [38] Markwardt C *et al.* 2002 *Astrophys. J* **575** L21–L24
- [39] Bradshaw C, Fomalont E and Geldzahler B 1999 *ApJ* **512** L121
- [40] Skrutskie M F *et al.* 2006 *The Astronomical Journal* **131** 1163–1183
- [41] Steeghs D and Casares J 2002 **568** 273–278 (*Preprint* astro-ph/0107343)
- [42] Abadie J *et al.* 2010 *NIM-A* **623** 223–240
- [43] Behnke B, Papa M and Prix R 2015 *PRD* **91** 064007
- [44] The LIGO Scientific Collaboration LALApps repository Web: <http://www.lsc-group.phys.uwm.edu/daswg/>